tvst

Article

Restoration of Vision and Retinal Responses After Adeno-Associated Virus–Mediated Optogenetic Therapy in Blind Dogs

Sergei Nikonov[1], Puya Aravand[1], Arkady Lyubarsky[1], Roman Nikonov[1], Angela J. Luo[1], Zhangyong Wei[1], Albert M. Maguire[1], Nicholas T. Phelps[1], Ivan Shpylchak[1], Keirnan Willett[1], Tomas S. Aleman[1], Rachel M. Huckfeldt[1], Pavitra S. Ramachandran[1], and Jean Bennett[1]

[1] Center for Advanced Retinal and Ocular Therapeutics (CAROT) and F.M. Kirby Center for Molecular Ophthalmology Scheie Eye Institute, University of Pennsylvania, Perelman School of Medicine, Philadelphia, PA, USA

Purpose: Optogenetic gene therapy to render remaining retinal cells light-sensitive in end-stage retinal degeneration is a promising strategy for treatment of individuals blind because of a variety of different inherited retinal degenerations. The clinical trials currently in progress focus on delivery of optogenetic genes to ganglion cells. Delivery of optogenetic molecules to cells in the outer neural retina is predicted to be even more advantageous because it harnesses more of the retinal circuitry. However, this approach has not yet been tested in large animal models. For this reason, we evaluated the safety and efficacy of optogenetic therapy targeting remaining diseased cone photoreceptors in the *Rcd1* dog model of retinitis pigmentosa.

Methods: Imaging and measures of retinal function and functional vision were carried out, as well as terminal studies evaluating multi-electrode array recordings and histology.

Results: Animals remained healthy and active throughout the study and showed improved retinal and visual function as assessed by electroretinography and visual-evoked potentials, improved navigational vision, and improved function of cone photoreceptors and the downstream retinal circuitry.

Conclusions: The findings demonstrate that an optogenetic approach targeting the outer retina in a blind large animal model can partially restore vision.

Translational Relevance: This work has translational relevance because the approach could potentially be extrapolated to treat humans who are totally blind because of retinal degenerative disease.

Introduction

The majority of inherited forms of blindness are caused by mutations that prevent proper development or function of retinal photoreceptors. There are now more than 270 different genes that have been identified that, if mutated, will lead to deterioration and loss of photoreceptors (https://sph.uth.tmc.edu/retnet/home.htm). Until recently, no treatments were available for inherited retinal degenerations, but with the recent approval of a gene augmentation therapy for disease caused by RPE65 deficiency (luxturna; voretigene neparvovec-rzyl),[1] other gene therapy reagents are being tested. Gene augmentation therapy requires that cells in the outer retina be viable. If the cells have died, this approach will not suffice. However, studies in rodent models have shown that gene transfer can be used to confer light sensitivity to remaining cells in the retina after photoreceptors have deteriorated.

In particular, ion channels derived from single-celled organisms have been successfully cloned and tested for their ability to restore vision in animal models of retinitis pigmentosa.[2]

The initial reports described effects of vision restoration in blind mice and showed that not only did optogenetic gene therapy reverse the electrophysiological and physiological deficits, but it also provided visually guided behavior.[3] Similar findings in rodents have been described after delivery of the optogenetic molecules through recombinant adeno-associated virus (AAV) vectors to either ganglion cells or to the outer retina (degenerating photoreceptors or bipolar cells).[2–8] Optogenetic gene therapy has also been tested in a few animal models with eyes closer in size and anatomical features to those of humans. The majority of these large animal studies targeted ganglion cells. Gaub et al.[9] delivered an AAV containing a modified mammalian ionotropic glutamate receptor (LiGluR) that acquired properties of a light-gated channel upon binding maleimide-azobenzene-glutamate 0 (MAG0(460)) through intravitreal injection to ganglion cells of the rod-cone dystrophy 1 (*Rcd1*) dog. They showed evidence of light responsiveness in tissue derived from these eyes. Ameline et al.[10] targeted a different canine model, the *RPE65*-mutant Swedish Briard, a model in which retinal function is lost well before there are structural changes. They showed that expression of their optogenetic molecules, channelrhodopsin and melanopsin, was durable in ganglion cells through 16 months and that there were no obvious structural or immunologic alterations. Although providing valuable information regarding the expression of optogenetic molecules in the large animal models of disease, outcomes regarding visual behavior were not provided in these studies.

The other studies described to date evaluated delivery in large animal or human-derived disease-free retinas. Sengupta et al.[11] treated ganglion cells in both (normal) macaque and human retinal explants ex vivo with AAV delivery and also showed multi-electrode array (MEA) evidence of light responsiveness specific to the optogenetic molecule, a red-shifted channel rhodopsin (ReAChR). Chaffiol et al.[12] expanded on these studies by characterizing inflammatory responses, as well as MEA responses (postmortem) in macaques injected intravitreally with AAVs containing Ca^{2+}-permeable channelrhodopsin (CatCh). McGregor et al.[13] used in vivo imaging in the living primate to measure ChrimsonR-evoked patterns of activity in retinal ganglion cells before and after acute loss of photoreceptor input. Near-infrared sensors have also been delivered through nonviral techniques in vivo in mice and in postmortem human retinas and shown to be functional.[14] Light responses were also measured from cone photoreceptors and retinal organoids derived from human-induced pluripotent stem cells treated with viral vectors containing any of a variety of different optogenetic molecules (eNpHR, Jaws, hCatCh, ChrimsonR and ReAChR).[8,15,16] These results, as well as dosing and safety data in normal-sighted nonhuman primates (NHPs), led to initiation of Phase I/II gene therapy clinical trials testing optogenetic therapy directed to ganglion cells in humans (www.clinicaltrials. gov: NCT02556736, NCT03326336, NCT04278131). Partial restoration of vision in one patient with end-stage retinitis pigmentosa was recently reported for one of these trials.[17] Restoration of vision in this patient was documented using three different psychophysical and neurophysiological tests. This study combined the use of gene delivery of an optogenetic molecule (ChrimsonR) with a device (goggles that relay the scene into light pulses designed to efficiently activate the optogenetically transduced retinal ganglion cells).

Development of optogenetic gene therapy targeting the outer retina offers a number of potential advantages compared to that targeting ganglion cells, including the facts that (1) by targeting outer retinal cells one can take advantage of the intact post-photoreceptor circuitry and computing power of the neural retina. This could potentially lead to higher quality vision; (2) because the AAV is diluted in a large volume in the vitreous cavity, higher titers must be used to be able to target sufficient numbers of retinal ganglion cells; (3) intravitreal injection exposes additional parts of the eye, including iris, lens epithelium, ciliary body, trabecular meshwork, corneal endothelium, and other parts of the body after going through the outflow track, to the recombinant virus; and (4) intravitreal injection of rAAV vectors often results in inflammatory and potentially harmful immune responses.[18–20] For these reasons, we evaluated the effects of optogenetic gene therapy after subretinal injection of an AAV serotype previously shown to target cone photoreceptors in NHPs after subretinal injection, AAV9.[16,21] We further ensured cone photoreceptor–specific expression by incorporating the cone arrestin (CAR) promoter to drive expression of the enhanced version of the optogenetic gene, NpHR (**e**NpHR),a light-gated hyperpolarizing chloride pump known as halorhodopsin that was originally isolated from a member of the Archaea family, *Natronobacterium pharaonis*. NpHR has a peak wavelength sensitivity of 580 nm[22] and the hyperpolarization that occurs after it is activated with light mimics the response of the normal photoreceptor cell. The eNpHR incorporates alterations in the NpHR sequence improving membrane localization.[23]

Busskamp et al.[3] had carried out optogenetic studies using eNpHR delivered by AAV2 in rodent models of retinal degeneration. The results were promising because there were numerous improvements in retinal and visual function in *rd1* mice. However, mice are not ideal targets for optogenetic studies because rodent eyes differ in many ways from those of large animals, including the fact that they have a much smaller percentage of cone photoreceptors, and they differ from large animals substantially with respect to AAV transduction characteristics and immune responses. Furthermore, mice are nocturnal and do not rely predominantly on vision to navigate. Furthermore, rd1 mice suffer a very fast retinal degeneration unlike humans with retinitis pigmentosa—the disease that rd1 mice model. Therefore, when 3 Rcd1 (*PDE6β*-mutant) dogs were made available to us in 2012, a time when AAV9.eNpHR was believed to be one of the most promising reagents, we initiated the studies described here. There is a relatively fast loss of rod photoreceptors in Rcd1 dogs and a slower loss of cone photoreceptors, similar to patients with retinitis pigmentosa. There are a number of advantages of carrying out studies in a large animal model with disease instead of using a healthy unaffected animal (NHP), including the fact that the presence of a full set of healthy photoreceptors in the NHP makes interpretation of physiological or behavioral assessments challenging.[12]

The field has progressed since 2012, with additional AAVs generated that can efficiently target cone photoreceptors in large animal models. For example, Khabou et al.[16] have described vector and promoter combinations that can target foveal cones from a subretinal approach (an AAV9 variant) or from a vitreal approach (AAV2-variant). Their studies took advantage of a red-shifted cruxhalorhodopsin, Jaws, developed and then initially tested by Chuong et al.[8] in rd1 mice. None of these reagents have been tested in the Rcd1 dog, and none have been used to test the effects on visual behavior in a large-animal model of retinal degeneration. Thus our studies using AAV9.NpHR in this naturally occurring large-animal model of retinitis pigmentosa provide useful insights into the functional and physiological potential of cone photoreceptor-directed optogenetic therapy.

The Rcd1 dog has an eye similar in size and anatomic features to the human. Furthermore, we were able to "age" the animals to get to a stage where a significant number of photoreceptors had already deteriorated. Although only primates have a cone-enriched fovea, dogs have an area centralis, a central region of the retina with an increased density of cone photoreceptors. As was shown by Pichard et al.,[24] by 3.5 years in the Rcd1 dog there are no remaining cone

photoreceptors except for a reduced number in the area centralis. Those that are present are histopathologically abnormal.[24] Here we report a partial reversal of retinal and visual function deficits in the *Rcd1* dog that correlate with definitively improved retinal function as assessed by different behavioral and electrophysiological tests. There was no evidence of inflammation in these animals either acutely or through up to 48 months of follow-up. The results provide the preclinical proof-of-concept data demonstrating that a one-time subretinal optogenetic gene therapy approach to the diseased cones of a large animal model can reverse blindness, thereby allowing improved navigation. Improvements in visual function correlated with electrophysiological findings. This work is thus translational in nature because it forms a bridge between basic research and (future) clinical care.

Methods

In Vivo Studies: Animals, Study Design and Ocular Surgery

Canines

The study was developed as reagents were purified and as mature large animals became available. The studies were in compliance with local and federal guidelines and were carried out under IACUC protocol 803871) and were in accordance with the ARVO Statement for the Use of Animals in Ophthalmic and Vision Research. Included were three dogs affected with rod-cone dystrophy caused by mutations in the beta subunit of rod phosphodiesterase 6 (PDE6β) (Table). These animals were homozygous for the *rcd1* nonsense mutation (G>A transition at nucleotide 2420 ; codon 807; Table). All animals were at least 13 months old before they were enrolled. After a baseline ophthalmoscopic evaluation, each animal received a unilateral subretinal (SR) injection of the study agent. One of the animals (Deino) received an intravitreal injection of AAV in the contralateral eye (Table). The contralateral eyes of the other animals were untreated. One untreated wildtype (WT) dog was used as a control for the visual behavior studies only.

The subretinal injection procedure was carried out using sterile instrumentation, surgical fields, injectable and topical medications. The subretinal injections were performed under direct visualization through an operating microscope after an anterior chamber paracentesis following procedures detailed elsewhere.[25–27] In brief, a needle was inserted through a trocar, introduced by sclerotomy, at the 2 or 10

Table. Summary of Procedures on Rcd1 Dogs

Name	Age at Intervention (mos)	Time Post/Age at ERG Testing (mos)	Time Post/Age at Y-Maze Testing (mos)	Time Post/Age at MEA (mos)	Retina ID	Retinal Studies	Treatment	Dose (vg)
Ginger	16	13/29	ND	18/34	a	ERG, MEA*	OD: Subretinally injected: AAV9.CAR-eNpHR	1.4E11
					b	ERG, MEA[†] ERG	OD: none OS: none	
Enyo	13	4/17	26/39	34/47	c	ERG, VEP, Y-Maze, OCT, MEA*	OS: Subretinally injected: AAV9.CAR.eNpHR	1.0E11
					d	ERG, VEP, Y-Maze, OCT, MEA	OD: none	
Deino	13	4/17	27/40	25/48	e	ERG, VEP, Y-Maze, MEA*	OS: Subretinally injected: AAV9.CAR.eNpHR	1.0E11
					f	ERG, VEP, Y-Maze	OD: Intravitreally exposed: AAV9.CAR.eNpHR	1.0E11

VG, vector genomes; OS, oculus sinister (left eye); OD: oculus dexter (right eye); ND, not done.

Measures: *area that was subretinally injected versus [†]area distant from the subretinally injected area.

o'clock position, which was then advanced through the vitreous to penetrate the retina in the posterior pole. Under microscopic control, 200 μL of the agent (resulting in doses of 1.0-1.4 E^{11} vector genomes) were injected into the subretinal space, thereby raising a dome-shaped retinal detachment (bleb). The solution was not drained but was resorbed within a few hours by the retina. The sclerotomy site was sutured with absorbable suture. The intravitreal injection was also carried out under microscopic control. After each procedure, a subconjunctival injection of 15 mg of Kenalog solution (40 mg/mL, 0.26 mL) was delivered, and the ocular surface was dressed with prednisolone acetate-gentamicin ointment (PredG, 0.3%/0.6%; Allergan Inc., Dublin, Ireland). Other than that, no immunosuppression was administered. Slit lamp examination and indirect ophthalmoscopy examinations were carried out before and immediately after subretinal injection, postoperative day 3 for each injection, every ~6 months, and before euthanasia.

Designated animals (Ginger, Enyo) were trained and tested for navigational abilities using a forced-choice Y-maze test.[28] For this, animals undergo a minimum of five days of training before carrying out scored tests. The training was carried out under bright light conditions (300 lux ambient illumination), and tests were carried out using both eyes and each eye individually. The latter was accomplished by applying an opaque ocular shield unilaterally. Once the animal was comfortable with the paradigm (was compliant about placement of opaque contact lenses and was comfortable with walking through the course to get to the other side of the room), he/she was dark adapted for 20 minutes and then given the formal tests.

For the formal testing, one eye (randomly selected) was tested at a time using a minimum of 20 trials per eye/light condition. A random number generator was

used to determine whether the light was switched on at the "arm 1" versus "arm 2" exit of the Y maze, with an equal number of 1s and 2s used during testing. The process was then repeated for the contralateral eye. Repeat testing was performed under the subsequent set of light conditions, again using 10 to 20 trials per condition/eye. The progression of testing conditions went from low to bright lighting. The room and Y-maze were cleaned with disinfectant to remove distracting smells before tests were initiated on another animal. The movements of the animal while in the light-tight maze were monitored using an infrared (FLIR ONE Pro; Teledyne FLIR, Thousand Oaks, CA, USA) thermal imaging camera. Scoring, measuring speed and accuracy in the navigation, was carried out by an experienced observer who was masked to the treatment paradigm. The definition for accuracy is making the correct choice to the arm of the maze that contains the light stimulus (i.e., the proportion of correct exit choices).[28] A paired-samples *t*-test was conducted to compare the ability of the animals to select the illuminated branch of the y-maze with the control eye versus the experimental eye.

Electroretinography (ERG) was carried out on three affected dogs treated with AAV9.CAR.eNpHR-YFP using modifications of procedures described by Ekesten et al.[29] Dogs were placed in the prone position on a custom-made support with the head hyperextended and situated inside a custom-made Faraday cage that was an $18' \times 18' \times 18'$ cubic aluminum chamber whose interior was completely covered with aluminum foil, serving to create a ganzfeld. Assemblies of LEDs mounted inside the ganzfeld served as light sources. The light sources were controlled by an Espion E2 System (Diagnosys LLC, Lowell, MA, USA), and the same system was used for ERG acquisition. Light sources were calibrated with an ILT500 photometer (International Light Technologies, Peabody, MA, USA). ERG scans were recorded with bipolar Burian-Allen electrodes (Hansen Labs, Coralville, IA, USA). Visual evoked potential (VEP) recordings were performed with Grass Gold Disc Electrodes (Grass Technologies, West Warwick, RI, USA). An active electrode was positioned occipitally, and a reference electrode was placed on the forehead. A ground electrode was placed on the left front leg of the animal. A topical anesthetic, 0.5% proparacaine, and mydriatic drugs, 2.5% phenylephrine and 1% tropicamide, were applied to both eyes. For ERG and VEP recordings, subjects were stimulated with sequences of 5 ms flashes delivered at one-second interstimulus intervals, and 200 to 400 individual responses were averaged for each intensity of stimulation.

All animals were followed up at least 1.5, years and two were followed up for more than two years after intervention (and close to four years of age; Table). At the termination of the study animals were euthanized, and samples were collected for MEA testing and histopathology.

Mice

Five retinas from four 2.5- to 3.5-month-old untreated C57BL/6 mice were studied to measure delays of population averaged On- and Off-responses. Retinas from dark-adapted mice were dissected under dim red light, and MEA recordings were done as described in Song et al.[30] The studies were in compliance with local and federal guidelines and were carried out under IACUC protocol 804282.

Study Agents

AAV9.CAR.eNpHR-YFP carries the enhanced halorhodopsin cDNA from Natronomonas (eNpHR) fused to the yellow fluorescent protein (YFP) reporter gene and driven by the CAR promoter. This construct, which includes a bovine growth hormone poly(A) has been previously described.[3] The AAV9 was manufactured by the Penn Vector Core (pennvectorcore.med.upenn.edu) at the University of Pennsylvania Perelman School of Medicine. AAVs were purified by density gradient ultracentrifugation and diafiltration in phosphate-buffered saline solution, passed through a 0.22-μm filter and stored frozen (−80°C) in sterile tubes until use.

Retinal

Spectral domain optical coherence tomography (SD-OCT; Spectralis, Imaging Heidelberg Engineering, Heidelberg, Germany) was used to obtain orthogonal radial volume scans and averaged B-scans of the central retina in the canine studies. The ONL was defined as the hypo-reflective band between the outer plexiform layer and the external limiting membrane. ONL thickness was measured within detectable regions of preserved ONL.

After euthanasia, eyes were enucleated, and retinas were dissected to isolate samples in defined locations of the retina for MEA. After MEA, samples were fixed in 4% paraformaldehyde in phosphate-buffered saline solution and cryosectioned for immunofluorescence and histopathologic studies. Cells expressing the eNpHR-YFP transgene were identified through immunofluorescence using Molecular Probes A1122 at 1:1000 or 1:500 dilutions. This is a polyclonal rabbit anti-GFP antibody, which cross-reacts with

YFP. Bipolar cells were identified using a mouse anti-Goα antibody (Millipore 3073; Millipore, Burlington, MA, USA) at 1:500 dilution. Cone matrix sheaths were labeled with peanut agglutinin (PNA-rhodamine, 1:250; Vector Laboratories, Burlingame, CA, USA). The secondary antibodies were Molecular Probes Alexa Fluor and were used at a dilution of 1:1000. Images were acquired on an Olympus FV1000 confocal microscope (Olympus, Tokyo, Japan).

Ex Vivo Studies: Multi-Electrode Array Recording

MEA recordings were performed with a 60 channel 200 μm interelectrode distance perforated array (60pMEA200/30iR-Ti; ALA Scientific Instruments, Inc., Farmingdale, NY, USA) using modifications of the previously reported techniques.[8,19] Briefly, retinal patches 5 mm in diameter were attached to cell culture membranes on the photoreceptor side with a gentle suction (using Corning 3460 Transwells with walls cut down to a height of 1 to 2 mm; Corning Inc., Corning, NY, USA). Membranes with retinas attached to them were cut out and the retinas were placed in the recording chamber ganglion cell side down. A harp (HSG-MEA-5BD; ALA Scientific Instruments, Farmingdale, NY, USA) was placed on top of the membrane to improve retinal contact with the electrodes. Retinas were perfused with oxygenated Ames solution (Sigma-Aldrich, St. Louis, MO, USA) maintained at 37°C and stimulated with calibrated flashes of 589 nm light. The data were sampled at 10 KHz and stored for further analysis using an MEA 1060-Inv amplifier (Multichannel Systems, Reutlingen, Germany), Windows computer, and PCI-6071E board controlled by the custom LabView-based software (National Instruments, Austin, TX, USA). Spike sorting was done using Plexon Offline Sorter (Plexon Inc., Dallas, TX, USA) and custom code developed in Matlab (MathWorks, Natick, MA, USA). Spike detection threshold was set at 4 SD and minimal inter-spike interval at 1 ms. Matlab-based coding was also used for all further analyses including calculation and quantification of firing rates and generation of raster plots. Publication quality figures were rendered using the export_fig utility.[31]

Results

Safety of Subretinal Optogenetic Therapy

We carried out serial eye examinations in canine subjects (anterior and posterior segment) and documented that there was no inflammation apparent at baseline or any timepoint post vector administration (Supplementary Fig. S6). Retinal examinations included indirect ophthalmoscopy and OCT imaging.

Subretinal delivery of optogenetic gene therapy was well tolerated in canine models with end-stage retinal degeneration. The alterations in the area covered by the retinal detachments and the subsequent flattening of the detachment could not be directly followed in the hours following the surgery due to animal care concerns. However, alterations in reflection of the tapetum caused by the detachment (as reported previously)[27] served as markers for the region exposed to AAV.YFP could not be detected ophthalmoscopically because of autofluorescence of the retina and a lack of appropriate filters to isolate YFP-specific wavelengths. There was no ophthalmoscopically detectable inflammation in any of the eyes/animals and no treatment-related changes in activity or well-being.

Visual Behavior

The WT control dog maintained normal visual behavior after intervention as judged subjectively by study staff when assessing his daily interactions with caretakers. Staff reported that animals taken outside of their runs avoided running into equipment (carts, cages, mops, etc.) when taken for daily enrichment in the hallways. Improved visual behavior (such as avoidance of obstacles) was reported subjectively by study staff for the three treated, affected animals (Ginger, Enyo and Deino) starting approximately one month after intervention and lasting through the duration of the study. Two of these animals (Enyo and Deino) underwent training for the forced choice Y-maze test, to compare visual responses using their AAV9.CAR.eNpHR-treated vs. untreated eyes. Both animals were able to navigate the maze correctly >95% of the time using their subretinally treated eye versus <50% of the time with their control eyes (Supplementary Fig. S1; $P = 0.033$) (Supplementary Video S1).

Electroretinograms

Bilateral ERGs were recorded from the three animals treated unilaterally with AAV9.CAR.eNpHR: Ginger, Deino, and Enyo. There were clear light-induced responses in the treated compared to the untreated (control) retinas, although, compared to WT dogs (whose cone ERG responses are ∼20 μV at the 3 cd s m^{-2} standard stimulus),[29] they required higher intensities of stimulation and were lower in magnitudes. Representative ERGs and VEP are shown in Figure 1.
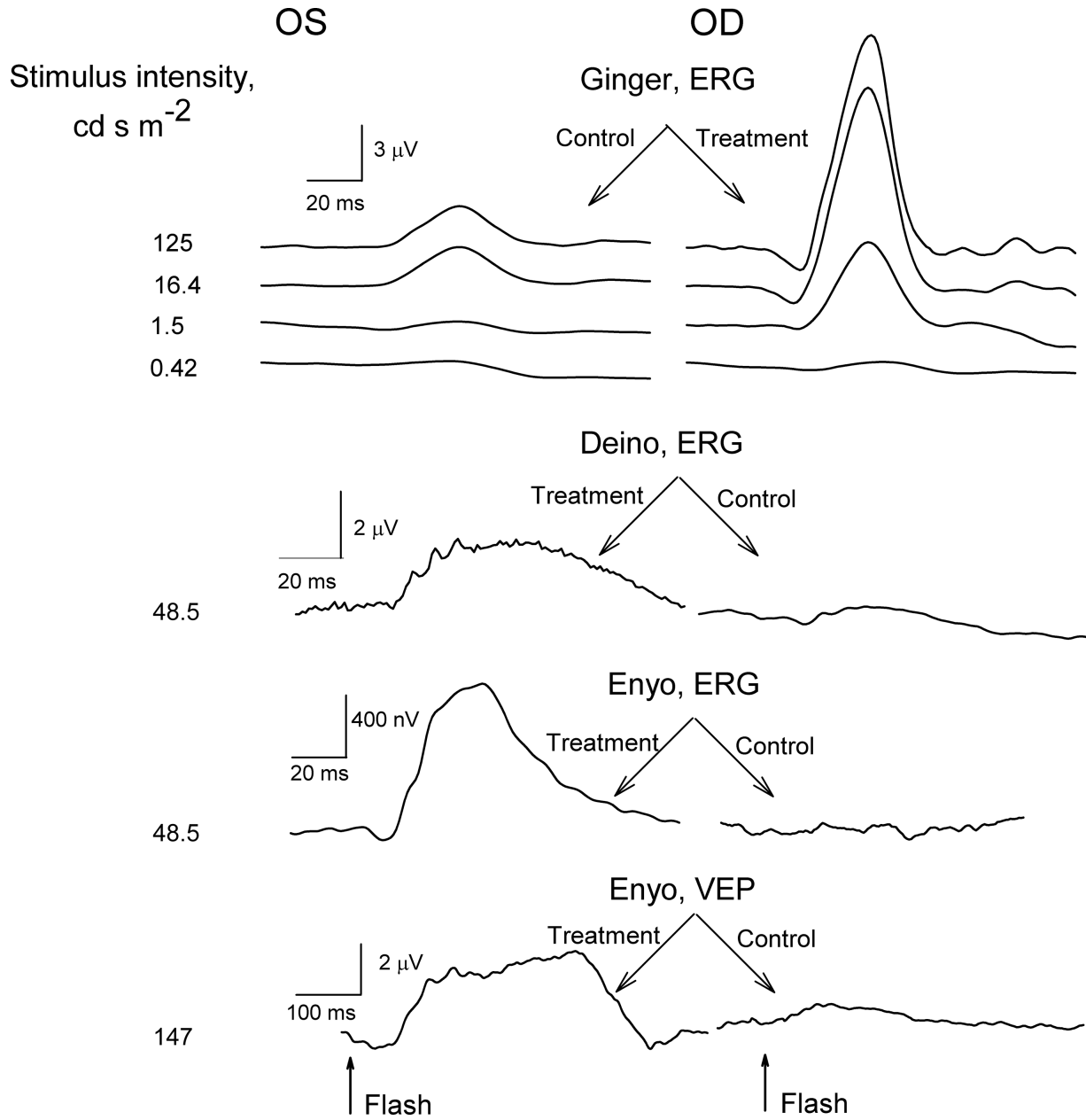
Figure 1. Light stimulation of the treated eyes results in robust ERG and VEP light responses that are significantly larger than responses driven by untreated retinas. ERGs elicited by a flash of a 125 cd s m^{-2} intensity from the left and right eye of the subject Ginger. ERGs elicited by a flash of a 48.5 cd s m^{-2} intensity from the left and right eyes, respectively, of the subjects Deino and Enyo. VEP elicited by a flash of a 147 cd s m^{-2} intensity from the left and right eyes, respectively, of the same subject (Enyo).

Multi-Electrode Array

All treated retinas demonstrated robust stable light responses at the brighter end of the intensity range (*retinas a, c, e*), whereas responses in the control untreated retinas (*retinas b, d, f*) were greatly diminished or completely abolished ([Figs. 2, 5](#), Supplementary Fig. S2). Note that Enyo had partially preserved native visual function as suggested by the rather strong responses to the first flash in a bright stimulation series observed in both threated and control retinas. However, although responses to the second and following flashes in the treated *retina c* demonstrated fast kinetics and stable amplitudes, responses in the control *retina d* under the same conditions had nearly disappeared (Supplementary Fig. S2). The very slow recovery of responses in the untreated retina can also explain the nearly undetectable ERG response from the Enyo's right eye ([Fig. 1](#)D): averaging responses to several hundred flashes as required by our ERG
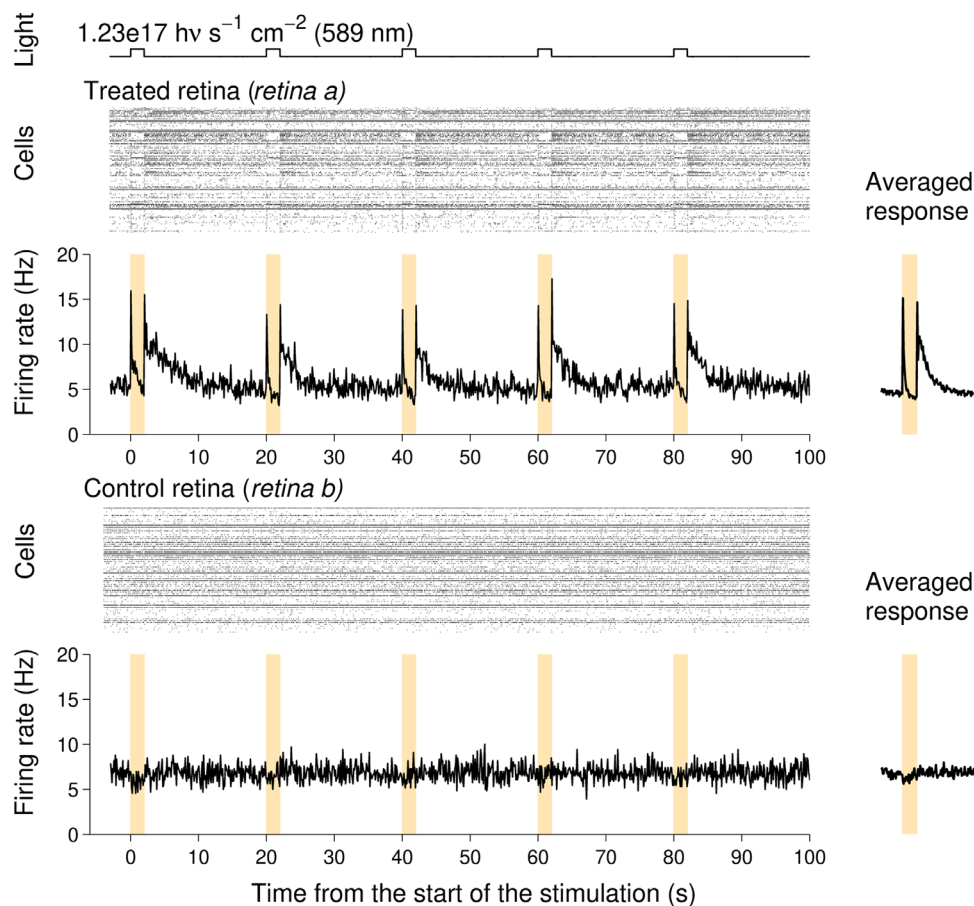
Figure 2.   eNpHR expression enables robust light responses in canine retinas. Graphs on the left show raster plots (labeled as "Cells") and per cell averaged firing rate traces recorded from the treated and untreated/control retinal samples of the same animal. In this particular example, treated and untreated retinal samples were obtained from the same retina by excising patches from the inside and outside of the injected area. On raster plots each *dot* corresponds to a spike firing event and each line represents firing from a particular cell. Firing rate traces were calculated using 100 ms time bin. *Upper trace* and *colored bars* indicate light stimulation time course. Per flash averaged (per flash per cell averaged) responses (titled "Averaged responses") are shown to the right of the corresponding (per cell averaged) firing rate traces.

protocol would result in a much diminished averaged response.

Firing rate traces presented in Figure 2 and Supplementary Figure S2 were calculated using a 100 ms time bin, which accounted for the relatively low noise levels and facilitated comparison of the responses from the treated and control retinas. To reveal fine details about bright flash response kinetics, firing rates for the treated retinas were also calculated using fast 5 ms and 2 ms time bins (Fig 3). Examining *retina a* responses plotted on a faster time scale demonstrated that its averaged Off-response had in fact two components, one with a high amplitude and very transient kinetics right after the flash offset, followed by a smaller and slower increase in the firing rate (Fig. 3A). On the level of individual cells, On-responses from this retina appear to show higher variability in the amplitudes and kinetics, whereas On-response latencies (time between flash

onset and response impetus) were similar across different On-cells and considerably slower compared to the fast Off-responses (Figs. 3B, 3C). Similar patterns were observed comparing responses from treated retinas in different animals. Although delays of the On-responses varied from 15 to 26 ms across different retinas (Fig. 3D), transient Off-responses from treated *retinas a* and *e* demonstrated nearly identical delays of around 7 ms (Fig. 3E). One treated retina (*retina c*) did not produce Off-responses during regular stimulation series though a much smaller Off-response could be detected during flicker stimulation. Because we do not have MEA light responses from the untreated WT canine retinas, we show normalized responses from a number of WT (untreated) adult murine retinas for comparison (Figs. 3F, G). In general, treated canine retinas demonstrated faster recovery kinetics for both On- and Off-responses, similar On-response latencies, and much shorter
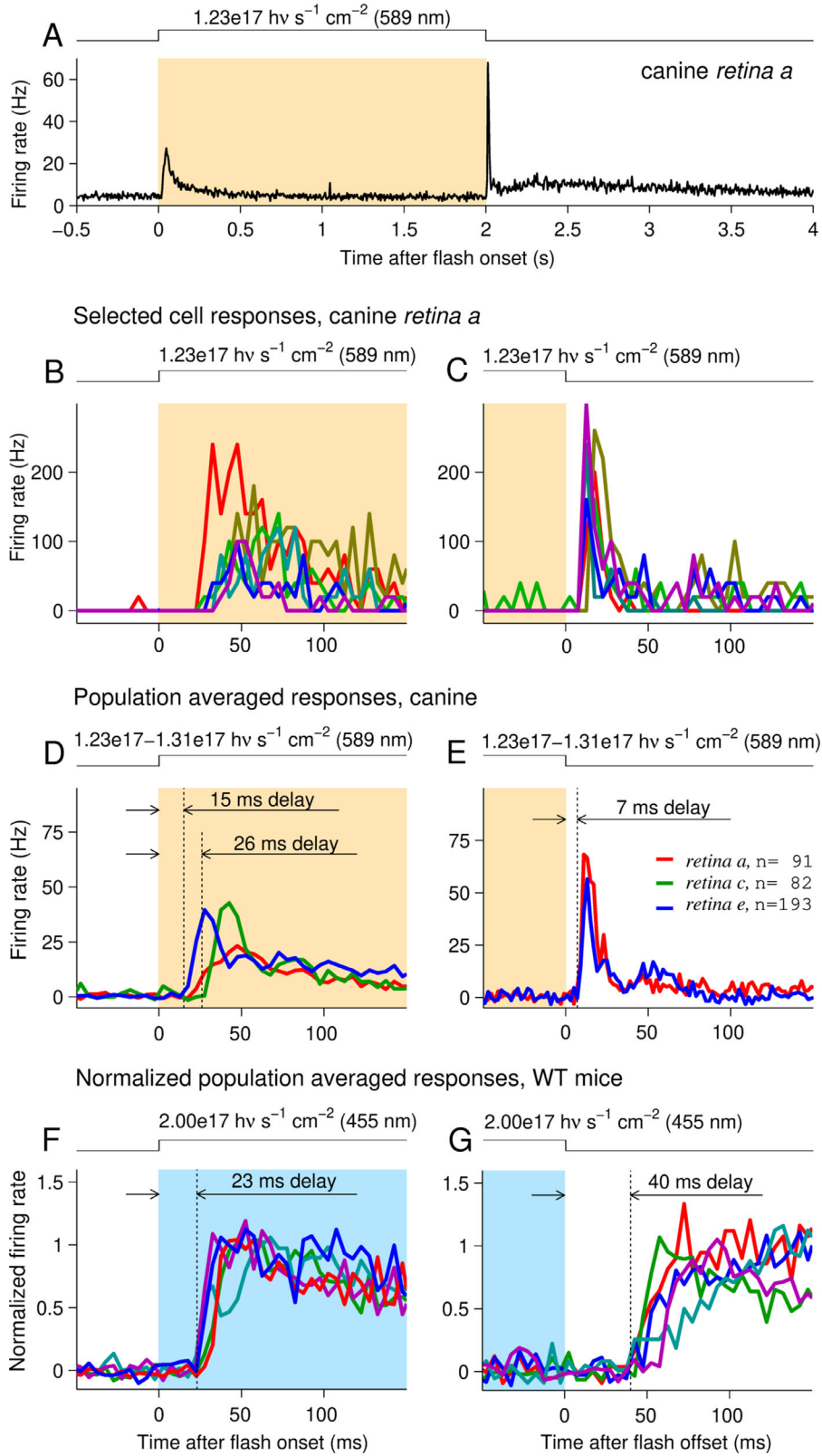
Figure 3. Off-responses in the eNpHR expressing retinas demonstrate unusually short delays while On-response latencies are consistent with the excitation of cone-driven pathway. Panel A plots an example of the per cell per flash averaged response obtained from one of the treated retinas (*retina a*), the Off-response is dominated by a very fast component followed by a slow decaying one. Panels B and C plot on a fast time scales examples of six On- and six Off-per flash averaged responses obtained from the individual cells identified in the *retina a*. Panels D and E plot per cell per flash averaged On- and Off-responses from all treated retinas, the color code and the total number of cells identified in each retina are given on the panel E. Panels F and G plot averaged responses from 5 different murine WT retinas (different colors

→

←

indicate different retinas). To facilitate comparison of response latencies observed from different mouse retinas, responses shown on panels F and G were normalized to the unity amplitude. The *dotted lines* in panels D–G indicate response latencies. Traces on panel E were calculated with 2 ms time bin, 5 ms time bin was used to calculate all other traces. Baseline firing (measured before flash onset for the On-responses and before flash offset for the Off-responses) had been subtracted from all traces except that from the panel A. All plotted responses were to standard two-second flashes. Note that Off-response for the *retina c* is not shown because that retina produced On-responses only during standard stimulation series. Traces above firing rate *graphs* and *colored bars* on the graphs indicate light stimulation events, flash intensities are given on the figure.

Off-response latencies compared to those observed in the WT murine retinas (15-26 ms vs. 23 ms, and 7 ms vs. 40 ms, respectively). More examples of On- and short-delayed Off-responses calculated using fast 2 ms time bin are presented in Supplementary Figure S3. Note that because of the increased noise in response traces calculated with a short time bin, only cells with larger responses were counted for the plots presented in this figure.

Both 455 nm light used in murine recordings and 589 nm light used in canine experiments were efficient in excitation of respective M-pigments. For murine S- and M-pigments 455 nm light efficiencies were around 0.3% and 50%, respectively. The 589 nm light, while approaching 100% efficiency in driving NpHR, was also around 90% efficient in exciting canine M-pigment and 7% efficient in S-pigment excitation.[29–33] Supplementary Figure S4 presents delay times measured in treated canine and WT murine retinas at different light intensities. Similar delays in canine and murine Off-responses might be expected if canine responses were driven by the activation of M-pigment or NpHR in cones (to facilitate comparison of the graphs murine data points were shifted along the x-axis to account for the efficiency of 455 light in M-pigment excitation). However, in the two treated canine retinas that generated Off-responses, the graphs reveal a clear shortening of the Off-response latencies compared to delays measured in WT murine retinas at intensities above 5e15 photons s^{-1} cm^{-2}. On the other hand— and consistent with the previous observations—On-response latencies were similar to those measured in WT retinas.

Analysis of individual cell responses in the treated canine retinas can identify populations of cells generating long-delayed Off-responses, similar to those observed in WT murine retinas and thus likely driven by cones. Interestingly, some cells appear to generate both short and long delayed Off-responses (Supplementary Fig. S5A). Of the three treated retinas studied in MEA experiments two (*retinas a* and *e*) produced both short-delayed and long delayed Off-responses. Manual counting of individual cell responses (calculated with either 2 ms or 5 ms time bin) demonstrated that the short-delayed component dominated

retina a Off-response (generated by ∼57% of the cells; see Figs. 3A, and 4). Around 15% of cells in this retina generated smaller long-delayed Off-responses, however the majority of those cells also produced typically larger short-delayed responses. Long-delayed component was more clearly defined in the *retina e* Off-response. Although short-delayed response again was a dominant component (generated by ∼37% of the cells), around 6% of *retina e* cells generated large predominantly long-delayed Off-responses, and 5% demonstrated comparable short- and long-delayed responses (Supplementary Fig. S5A). About 22% of cells in *retina a* produced yet another type of the Off-response, a very slow one peaking at around 400 ms after flash offset. This response may or may not follow short-delayed component (Supplementary Fig. S5B). In *retina e* such slow responses were generated by less than 3% of cells.

Population analysis also demonstrates that On-, On/Off-, and Off-subpopulations of ganglion cells can be identified in the eNpHR-treated retinas, at least at the brightest intensities (Fig. 4). The fractions of cells producing On, On/Off- and Off-responses were around 7%, 26% and 31% for *retina a*, and around 12%, 23% and 13% for *retina e* respectively (counting together all types of Off-responses). As was mentioned earlier, *retina c* produced On-responses only.

To estimate light sensitivity, we measured response amplitude for each cell and tracked its changes throughout the intensity range. Response amplitudes below three standard deviations of the baseline were accepted to be within noise and such responses were not counted. The upper two rows of Fig. 5 (panels A to F) give examples of histograms counting responding cells for *retina a* at three different light intensities (responding cells were counted starting with the second histogram bin, numbering bin centered at zero as a zero-bin). To facilitate measurements of responses of multiple cells at many different intensities, their firing rates were calculated with a 100 ms time bin. This reduced noise of firing rate versus time traces and simplified detection of somewhat slower On-responses. At the same time, it reduced calculated peak amplitudes of responses with fast kinetics, resulting in a lower count of the number of the cells producing
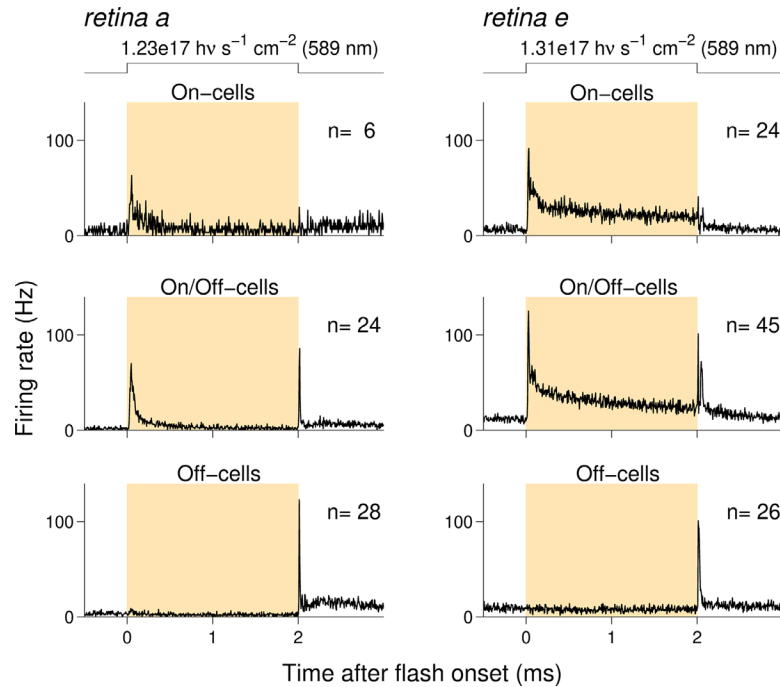
Figure 4. On-, On/Off-, and Off-cells can be identified in the eNpHR expressing retinas. Per cell per flash averaged responses of manually selected (non-overlapping) subpopulations of cells in *retinas a* and *e* were calculated using 5 ms time bin. Numbers of cells in each subpopulation are given on the graphs. Traces above firing rate *graphs* and *colored bars* on the graphs indicate light stimulation events, flash intensities are given on the figure.

fast short delayed Off-responses. Thus, for *retina a*, manual inspection of individual cell responses calculated with fast time bins gives a fraction of On- and all types of Off-responding cells around 33% (7 (On) + 26 (On/Off) = 33%) and 57% (26 (On/Off) + 31 (Off) = 57%), respectively, compared to 40% and 54%, which can be obtained from the data presented on Figure 5, panels C, F. Reported Off-response amplitudes include measurements from all types of Off-responses when Off-responses consisted of several components, the amplitude of the largest component was measured. The per-cell averaged response amplitude (counting all cells in the retina), fraction of responding cells, and per responding cell amplitude (counting light sensitive cells only) as functions of light intensity for all treated and for corresponding control retinas are given on the lower two rows of panels on Figure 5 (panels G, H, I for the treated and J, K, L for untreated retinas). The graphs demonstrate strong increases in response amplitudes and number of responding cells in the treated retinas at intensities above 1e15-1e16 photons s^{-1} cm^{-2}. As was noted above, elevated measurements for the control *retina d* and, at medium intensities, for the treated *retina c* suggest partial preservation of the regular cone function in these retinas. The intensity-dependent increase in the "per responding cell" response ampli-

tude (the total amplitude measured from all counted On- or Off-responding cells divided by the corresponding cell count) shows that the increase in total response amplitude was due to both the increased number of responding cells and increased responses of the individual cells.

Treated retinas also demonstrated strong responses to the 4 Hz flicker stimulation. *Retina e* had mainly On- flicker response with a smaller Off-response gradually disappearing as stimulation series progressed (Fig. 6). On-responses of *retinas a* and *c* disappeared soon after the start of the flicker series while their fast Off-responses (robust response for *retina a* and a small response for *retina c*) were observed throughout the stimulation (data not shown).

Retinal Structure

Locations of subretinal injection were readily identified through alterations in the appearance of the underlying tapetum. Such changes in reflectivity have been described previously.[27,32–34] OCT studies revealed focally severe disease with abrupt transitions in thickness (Supplementary Fig. S6), a phenotypic feature of *PDE6B*-associated retinal degeneration in dogs.[25] There are no overt signs of intraocular inflammation
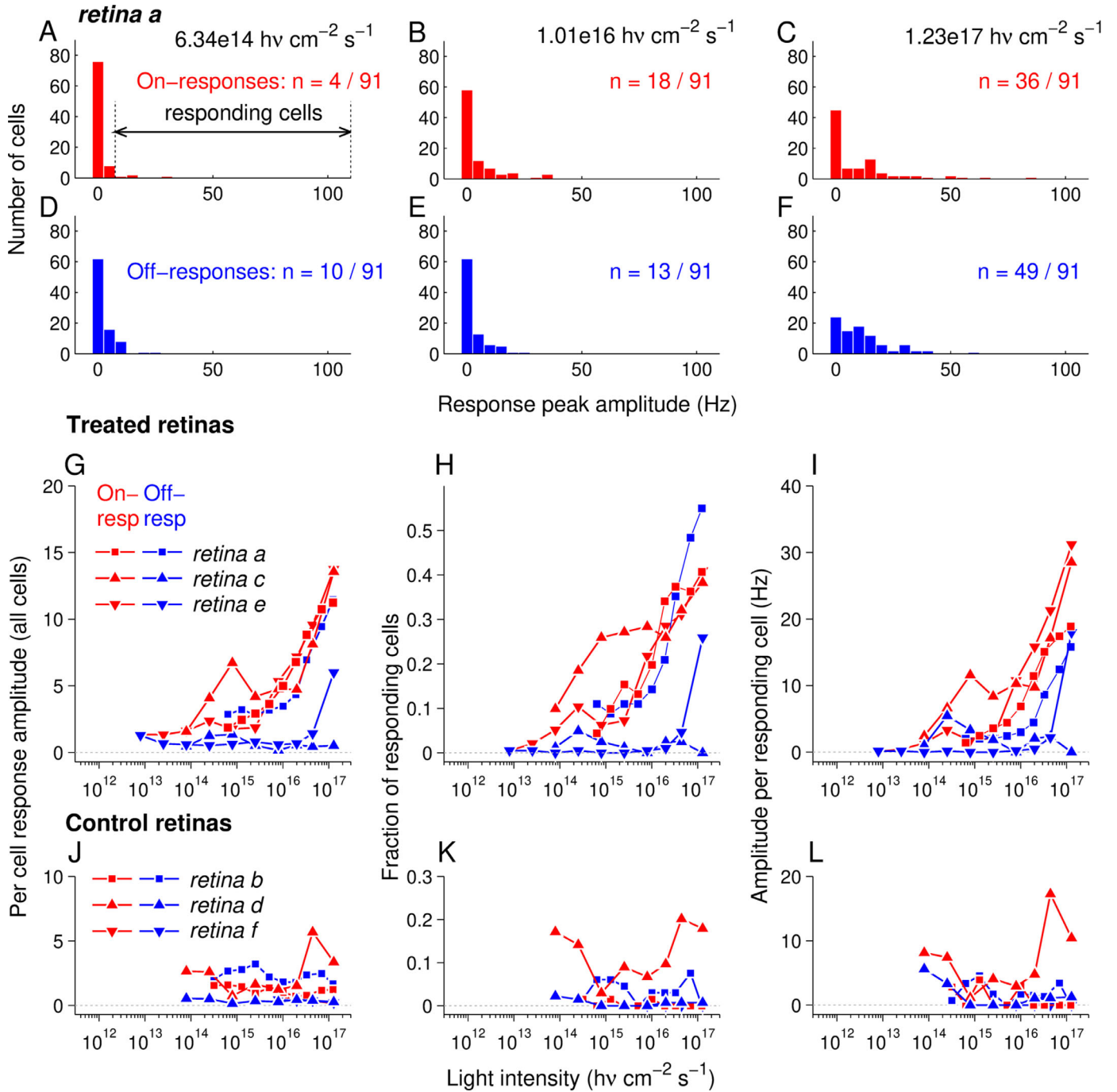
Figure 5.   The eNpHR expressing retinas demonstrate sharp increase in the response amplitude and the number of light-sensitive cells at the brighter end of the intensity range. Firing rates of the individual cells in each retina were calculated using 100 ms time bin. For each cell On-response amplitude was measured as a peak firing rate after flash onset minus averaged firing rate before flash onset, and Off-response amplitude as a peak firing rate after flash offset minus averaged firing rate before flash offset. Cells producing responses with amplitudes below 3 SD of the pre-flash baseline were counted as non-responding. Histograms at the upper part of the figure (panels A–F) give numbers of cells producing responses in a particular range of amplitudes at three different intensities for *retina a* (On- and Off-responses were independently counted so that ON/Off-cells would be counted in both On and Off-categories, the width of the histogram bin is 5 Hz). Cells in the second and higher bins (counting bin centered at zero as zero-bin), that is those with responses above 7.5 Hz were counted as light sensitive. Flash intensities, numbers of responding cells and total number of cells identified in the retina are given on the graphs. Plots on the lower part of the figure illustrate dependence on the flash intensity of the following parameters: (1) per cell per flash averaged response amplitudes counting all cells in the retina (panels G, J), (2) fraction of responding cells (panels H, K), and (3) per cell per flash averaged amplitudes counting light-sensitive cells only (panels I, L). The data for the treated retinas is plotted on panels G–I and for the corresponding control/untreated retinas on panels J–L. The symbol and color keys are given on the figure.
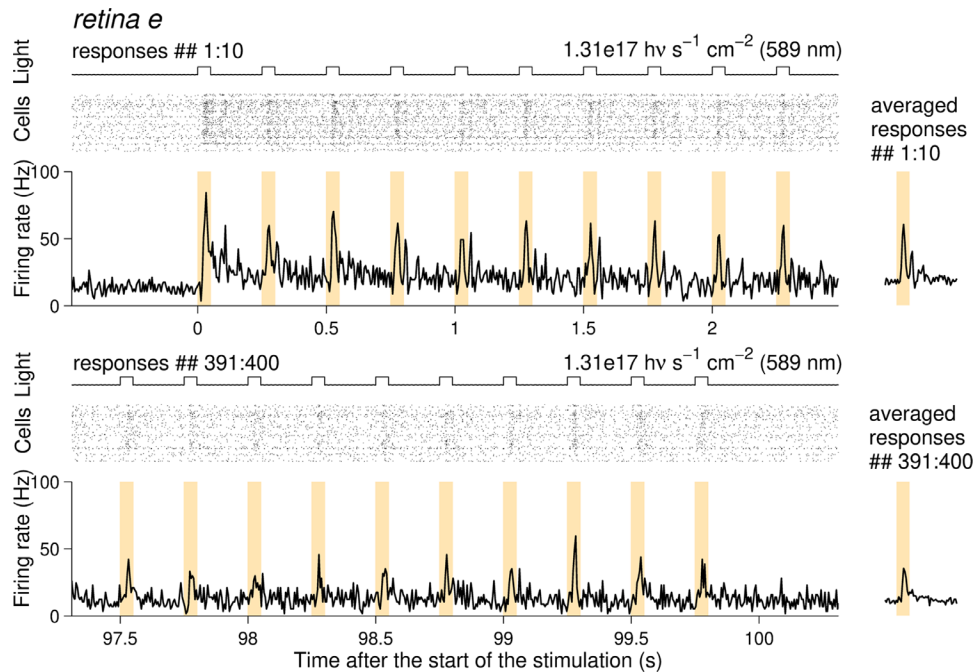
Figure 6. The eNpHR-expressing retinas produce robust response to the flicker stimulation. Raster plots, per cell averaged, and per cell per flash averaged (labeled as "averaged responses") firing rates of the *retina e* for the first (upper half of the figure) and last (lower half of the figure) 10 flashes in a flicker stimulation series. Stimulation series included four hundred 50 ms flashes delivered at 4 Hz. Firing rates were calculated using 5 ms time bin. *Traces* above raster plots and *colored bars* on the firing rate plots indicate light stimulation events.

such as images suggestive of vitreous cells, intraretinal or subretinal infiltrates or granulomas. There are no differences between injected and uninjected portions of the retina.

Histopathologic analyses revealed severe retinal degenerative changes throughout both the treated and the control retinas of the Rcd1 animals (not shown). The retinas lacked outer segments, the outer nuclear layers were significantly reduced in thickness, and there were occasional dislodged or hypertrophic RPE cells and some rosettes in the regions that had received subretinal injection. Immunofluorescence studies showed that the majority of residual cone photoreceptors bodies in the region of the subretinal injection expressed the transgene (Supplementary Fig. S7). Cone terminals remained intimately associated with the dendritic processes of bipolar cells identified by Goα staining. No rod photoreceptors were observed. There were no inflammatory cells present save for rare macrophages.

Discussion

This is the first demonstration to our knowledge of successful amelioration of retinal function *and* functional vision in a large animal model using optogenetic gene therapy to deliver the optogenetic gene to diseased cone photoreceptors. By targeting cone photoreceptors (instead of cells in the inner retina or retinal ganglion cells themselves), one can theoretically take advantage of the greater convergence in downstream retinal ganglion cells (RGCs).

Improvements in functional vision (navigation) correlated with improved retinal function as assessed by ERGs in subretinally treated (but not control) eyes. Judging by their shape and time course, ERG signals recorded from treated eyes represent cone-driven b-waves generated by cone on- bipolar cells. The signals presented in Figure 1 peak at ∼40 ms; similar to cone b-waves recorded from normal dogs, which peak at ∼35 ms whereas the rod-driven b-waves peak at ∼80 to 90 ms.[29] VEP records prove that light-evoked retinal electric activity reaches the visual cortex, a conclusion also supported by the visual behavior data. Images obtained with noninvasive imaging showed no features typically associated with inflammation and thus gave assurance of the long-term safety of the approach.

In the MEA tests, treated retinas (but not controls) demonstrated both Off and On-responses attributable to eNpHR activity. Finally, histologic analyses revealed durable expression of the transgenes in the targeted cone photoreceptors. Importantly, subretinal delivery and expression of the optogenetic molecule in cone photoreceptors was well tolerated and was safe.

Of the measures used in the current study, perhaps the most objective data demonstrating efficacy of this approach come from MEA measurements. The eNpHR-treated retinas showed fast short delayed Off-responses which can be confidently described as eNpHR-driven. This conclusion is supported by several lines of evidence: (1) no comparable responses were observed in the control (untreated or intravitreally injected) retina samples, (2) there was a sharp increase in the slope of the response intensity curve above 1e16 photons s^{-1} cm^{-2}, and (3) the very short 7 ms delay of the Off-responses suggests that the responses originate in the cells downstream from the photoreceptors. Note also that responses of this type were not observed in WT murine retinas.

Observation of On-responses in the treated but not control retinas and similarity of response-intensity dependences of On- and eNpHR-driven fast Off-responses suggests that at least at the brighter end of the intensity scale (above 5e15 photons s^{-1} cm^{-2}), On-responses were also eNpHR driven. The strong acceleration of bright flash recovery kinetics observed for the On-responses in the treated canine retinas as opposed to On-responses in the WT murine retinas is also consistent with the above conclusion. At the same time, similarity of On-response latencies in the treated canine retinas to those of cone-driven On-responses suggests that On-responses in the treated canine retinas originated in cones. The sharp increase in the total retinal response amplitude at the brighter intensities detected in MEA experiments appears to be caused by both the increase in the number of light-sensitive cells and the increase in the amplitudes of the individual cell responses.

Although short-delayed Off-responses most likely result from the off-target expression of the eNpHR (which might be a consequence of retinal remodeling, see below), they can serve the useful function of increasing the amount of information sent from the retina to the brain. Such off-target expression also appears to enhance the retina's ability to respond to the higher frequency stimuli.

The results extend those previously reported by Busskamp et al.,[3] who delivered a similar construct to cone photoreceptors in blind mice using AAV2. Here we used AAV9, which is far more efficient in targeting cone photoreceptors in retinas of large animal models.[21] The cone-specific promoter, CAR, further insured expression restricted to the target cells. The intervention was durable as shown by strong MEA responses in treated retinas through at least four years after intervention. Success of the intervention depends on presence of viable (even if diseased) cone photoreceptors and the ability to target them. Because only 3% of photoreceptors in mouse retinas are cones, it is more challenging to do comparative studies of cone cell targeting in this species.[35]

The positive results in this study beg consideration of further developing cone-directed optogenetic therapy for retinal degeneration. There are a number of findings in the current study which may help guide the next steps. First, the experience to date in in vivo laboratory studies uses two different animal models of retinitis pigmentosa, both of which suffer from *Pde6β* deficiency: the rd1 mouse (Busskamp et al.[3]) and the Rcd1 dog, as described here. Perhaps *PDE6β* is uniquely tractable with cone-directed optogenetic therapy? Would similar results be elicited in other genetic forms of retinitis pigmentosa? Further studies in animal models of other inherited retinal degenerations (particularly large animals) would be informative given the anatomical features and similar surgical approaches used in canines and humans. Naturally occurring canine models have been described in > 100 breeds and with at least 12 different disease-causing genes.[36] Second, delivery vehicles and constructs must be further optimized. There have been numerous improved optogenetic molecules generated that are responsive to lower intensity light and different wavelengths and those will enhance safety of the approach. The AAV armamentarium has grown similarly, and there are now a number of highly-specific retinal cell promoters available. Even with the proximity afforded by subretinal injection, only a few of the AAV serotypes described to date target cone photoreceptors efficiently. As examples, neither AAV2 nor AAV8 transduce cone photoreceptors efficiently after subretinal injection of low doses of AAV in non-human primates.[21,26] Thus subretinal delivery of the AAV vector, as was done in the present study, was required. Notably, we showed that delivery of the reagent through a route that does not expose cone photoreceptors (intravitreal injection) did not result in rescue. It has been a challenge to identify AAV serotypes that lead to efficient transduction of an area equivalent to the (primate) cone photoreceptor-enriched macula after intravitreal injection in large animals.[20] Intravitreal delivery can, however, target the foveal ganglion cells on the rim of the foveal pit.[37] McGregor et al.[13] used intravitreal delivery of ChrimsonR and the calcium indicator GCaMP6s using dual AAV2 vectors to demonstrate optogenetic responses of ganglion cells in non-human primates. Measurements were made through adaptive optics scanning light ophthalmoscopy calcium imaging before and after ablation of the fovea. The ability to delivery optogenetic therapy to cone photoreceptors through intravitreal injection would change what would currently

be an operating room procedure into an office procedure.

The work by Khabou et al.[16] using novel AAV capsid-promoter combinations provides further promise. Their studies demonstrate that it is possible to successfully target cone photoreceptors through both subretinal and intravitreal routes of administration. Khabou et al.[16] showed that subretinal delivery of AAV7m8, as well as a rationally designed variant of AAV9, AAV9-7m8, along with a transgene driven by a 1.7 red opsin enhance/promoter sequence transduces the fovea, as well as more distal cone photoreceptors after subretinal injection. (Intravitreal injection of these variants also served to transduce cone photoreceptors, although not as efficiently as subretinal injection.) AAV9-7m8 has the additional advantage that it appears to diffuse laterally after peripheral injection and thus can transduce the fovea even after delivery of the AAV to the peripheral retina. Khabou et al.[16] used this vector to demonstrate robust optogenetic light responses in tissue explants after subretinal delivery of AAV9-7m8.PR1.7-Jaws-GFP, in NHPs. Jaws, a red-shifted crux halorhodopsin derived from Halobacterium, had been previously described by Chuong et al.[8] and shown in tissue explants from Pde6β−/− (rd1) mice to mediate higher ganglion cell spiking rates than other optogenetic molecules. This reagent promises to be useful to test optogenetic restoration of functional vision in vivo in large animal models with retinal disease and, of course, ultimately humans with retinal disease; Finally, additional studies involving optogenetic therapy should further query the effects of retinal remodeling. There may have been some evidence in our study that the remodeling that is known to occur in retinal degeneration affected the ability of eNpHR to drive the cone-driven pathway. Retinal remodeling could be disadvantageous in terms of reducing the signal/noise ratio.

A 36 ms delay in the Off-responses of some cells in the treated retinas (close to 40 ms delays observed in the WT murine retinas), indicates that those responses were driven by the surviving cones (either cones with partially preserved outer segments or more likely by NpHR expressing ones). However, because some of the RGCs generated both short-delayed and long-delayed Off-responses, it is possible that eNpHR can interfere with the cone-driven pathway. Remodeling can affect retinal structure, synaptic contacts, dendritic processes, protein trafficking, and expression patterns.[38,39] Alternatively, perhaps the remodeling affected AAV transduction patterns and allowed the AAV to express in cells that are not cone photoreceptors. Analysis of individual RGC responses suggests that On-, Off-, and On/Off-cells can be present in the treated retinas, although On- and short delayed Off-responses likely originate in different retinal cells upstream of RGCs. We could not identify any transduced cells other than cone photoreceptors using immunofluorescence; however, that technique may not have been sensitive enough to detect low levels of expression.

In circumstances where retinas are completely devoid of photoreceptors, it may be possible to harness bipolar cells and the circuitry downstream from those cells. Successful targeting of bipolar cells of blind mice using such a strategy was first demonstrated by Lagali et al.[5] using AAV2. An AAV targeting bipolar cells, AAVBP2, was designed by directed evolution by Cronin et al.[4] and has a good safety profile in normal-sighted non-human primates.[14] Cronin et al.[4] demonstrated that it is indeed possible to use this AAV to transduce bipolar cells and achieve rescue of retinal function in blind mice. Other groups have successfully used other engineered AAVs to target optogenetic molecules to bipolar cells in blind mice using intravitreal or subretinal injection.[7,40,41] One of the challenges of a bipolar targeting strategy in end-stage blindness is the same as described above: changes in the retinal circuit over time,[2] likely because of the remodeling that occurs during the degenerative process.[42,43]

The MEA responses in the current study appear at lower stimulus intensities than those reported in earlier optogenetic therapy applications where channelrhodopsin 2 was delivered to the On- bipolar cells in mice using a tyrosine mutant AAV capsid and a bipolar cell promoter.[44] Here, we see responses at (3-10)E15 photons s^{-1} cm^{-2} in dogs versus the 4E+16 photons s^{-1} cm^{-2} threshold reported by Doroudchi et al.[44] There are many variables that could account for this discrepancy. Perhaps we more efficiently targeted the remaining retinal cones (through the AAV9 and cone arrestin promoter) rather than downstream neurons (done by Doroudchi et al.[44]). However, by moving the target of treatment from bipolar cells (as done by Doroudchi et al.[44]) to photoreceptors (as done here), one might expect a greater signal convergence in the retinal ganglion cells.

In summary, the recent progress in engineering optogenetic molecules that respond optimally to light intensities and wavelengths that are typically encountered in daily living (i.e., less intense and shorter wavelengths of light) and with faster kinetics offers great promise to patients totally blind due to retinal degenerative diseases. The data presented here support further studies evaluating the safety and efficacy of cone photoreceptor-directed optogenetic therapy. This could be carried out in conjunction with image intensifiers (i.e., goggles) that deliver the appropriate light stimuli to the treated eye as was recently successfully carried out by Sahel and colleagues[17] in studies of optogenetic therapy targeting ganglion cells.

Acknowledgments

References

1. Russell S, Bennett J, Wellman JA, et al. Efficacy and safety of voretigene neparvovec (AAV2-hRPE65v2) in patients with RPE65-mediated inherited retinal dystrophy: a randomised, controlled, open-label, phase 3 trial. *Lancet.* 2017;390:849–860.

2. Busskamp V, Picaud S, Sahel JA, Roska B. Optogenetic therapy for retinitis pigmentosa. *Gene Ther.* 2012;19:169–175.

3. Busskamp V, Duebel J, Balya D, et al. Genetic reactivation of cone photoreceptors restores visual responses in retinitis pigmentosa. *Science.* 2010;329:413–417.

4. Cronin T, Vandenberghe LH, Hantz P, et al. Efficient transduction and optogenetic stimulation of retinal bipolar cells by a synthetic adeno-associated virus capsid and promoter. *EMBO Mol Med.* 2014;6:1175–1190.

5. Lagali PS, Balya D, Awatramani GB, et al. Light-activated channels targeted to ON bipolar cells restore visual function in retinal degeneration. *Nat Neurosci.* 2008;11:667–675.

6. Tomita H, Sugano E, Yawo H, et al. Restoration of visual response in aged dystrophic RCS rats using AAV-mediated channelopsin-2 gene transfer. *Invest Ophthalmol Vis Sci.* 2007;48:3821–3826.

7. Mace E, Caplette R, Marre O, et al. Targeting channelrhodopsin-2 to ON-bipolar cells with vitreally administered AAV Restores ON and OFF visual responses in blind mice. *Mol Ther.* 2015;23:7–16.

8. Chuong AS, Miri ML, Busskamp V, et al. Noninvasive optical inhibition with a red-shifted microbial rhodopsin. *Nat Neurosci.* 2014;17:1123–1129.

9. Gaub BM, Berry MH, Holt AE, et al. Restoration of visual function by expression of a light-gated mammalian ion channel in retinal ganglion cells or ON-bipolar cells. *Proc Natl Acad Sci USA.* 2014;111:E5574–5583.

10. Ameline B, Tshilenge KT, Weber M, et al. Long-term expression of melanopsin and channelrhodopsin causes no gross alterations in the dystrophic dog retina. *Gene Ther.* 2017;24:735–741.

11. Sengupta A, Chaffiol A, Mace E, et al. Red-shifted channelrhodopsin stimulation restores light responses in blind mice, macaque retina, and human retina. *EMBO Mol Med.* 2016;8:1248–1264.

12. Chaffiol A, Caplette R, Jaillard C, et al. A New Promoter Allows Optogenetic Vision Restoration with Enhanced Sensitivity in Macaque Retina. *Mol Ther.* 2017;25:2546–2560.

13. McGregor JE, Godat T, Dhakal KR, et al. Optogenetic restoration of retinal ganglion cell activity in the living primate. *Nat Commun.* 2020;11:1703.

14. Nelidova D, Morikawa RK, Cowan CS, et al. Restoring light sensitivity using tunable near-infrared sensors. *Science.* 2020;368:1108–1113.

15. Garita-Hernandez M, Guibbal L, Toualbi L, et al. Optogenetic Light Sensors in Human Retinal Organoids. *Front Neurosci.* 2018;12:789.

16. Khabou H, Garita-Hernandez M, Chaffiol A, et al. Noninvasive gene delivery to foveal cones for vision restoration. *JCI Insight.* 2018;3(2):e96029.

17. Sahel JA, Boulanger-Scemama E, Pagot C, et al. Partial recovery of visual function in a blind patient after optogenetic therapy. *Nat Med.* 2021;27:1223–1229.

18. Dalkara D, Byrne LC, Klimczak RR, et al. In vivo-directed evolution of a new adeno-associated virus for therapeutic outer retinal gene delivery from the vitreous. *Sci Transl Med.* 2013;5:189ra176.

19. Cukras C, Wiley HE, Jeffrey BG, et al. Retinal AAV8-RS1 gene therapy for X-linked retinoschisis: initial findings from a phase I/IIa trial by intravitreal delivery. *Mol Ther.* 2018;26:2282–2294.

20. Ramachandran PS, Lee V, Wei Z, et al. Evaluation of dose and safety of AAV7m8 and AAV8BP2 in the non-human primate retina. *Hum Gene Ther.* 2017;28:154–167.

21. Vandenberghe LH, Bell P, Maguire AM, et al. AAV9 targets cone photoreceptors in the nonhuman primate retina. *PLoS One*. 2013;8:e53463.
22. Zhang F, Wang LP, Brauner M, et al. Multimodal fast optical interrogation of neural circuitry. *Nature*. 2007;446:633–639.
23. Gradinaru V, Thompson KR, Deisseroth K. eNpHR: a Natronomonas halorhodopsin enhanced for optogenetic applications. *Brain Cell Biol*. 2008;36:129–139.
24. Pichard V, Provost N, Mendes-Madeira A, et al. AAV-mediated gene therapy halts retinal degeneration in PDE6beta-deficient dogs. *Mol Ther*. 2016;24:867–876.
25. Bennett J, Anand V, Acland GM, Maguire AM. Cross-species comparison of in vivo reporter gene expression after recombinant adeno-associated virus-mediated retinal transduction. *Methods Enzymol*. 2000;316:777–789.
26. Bennett J, Maguire AM, Cideciyan AV, et al. Recombinant adeno-associated virus-mediated gene transfer to the monkey retina. *Proc Natl Acad Sci USA*. 1999;96:9920–9925.
27. Acland GM, Aguirre GD, Ray J, et al. Gene therapy restores vision in a canine model of childhood blindness. *Nat Genet*. 2001;28:92–95.
28. Aravand P, Ramachandran PS, Schpylchak I, Phelps NT, Nikonov S, Bennett J. Protocols for visually guided navigation assessment of efficacy of retina-directed cell or gene therapy in canines. *Front Neurosci*. 2017;11:215.
29. Ekesten B, Komaromy AM, Ofri R, Petersen-Jones SM, Narfstrom K. Guidelines for clinical electroretinography in the dog: 2012 update. *Doc Ophthalmol*. 2013;127:79–87.
30. Song JY, Aravand P, Nikonov S, et al. Amelioration of neurosensory structure and function in animal and cellular models of a congenital blindness. *Mol Ther*. 2018;26:1581–1593.
31. Altman Y. export_fig. Available at: https://github.com/altmany/export_fig/releases/tag/v3.25 GitHub; Accessed May 17, 2022.
32. Acland GM, Aguirre GD, Bennett J, et al. Long-term restoration of rod and cone vision by single dose rAAV-mediated gene transfer to the retina in a canine model of childhood blindness. *Mol Ther*. 2005;12:1072–1082.
33. Bennicelli J, Wright JF, Komaromy A, et al. Reversal of blindness in animal models of leber congenital amaurosis using optimized AAV2-mediated gene transfer. *Mol Ther*. 2008;16:458–465.
34. Jacobs G, Deegan J, Crognale M, Fenwick J. Photopigments of dogs and foxes and their implications for candid vision. *Vis Neurosci*. 1993;10:173–180.
35. Wang YV, Weick M, Demb JB. Spectral and temporal sensitivity of cone-mediated responses in mouse retinal ganglion cells. *J Neurosci*. 2011;31:7670–7681.
36. Beltran WA. The use of canine models of inherited retinal degeneration to test novel therapeutic approaches. *Vet Ophthalmol*. 2009;12:192–204.
37. Dalkara D, Kolstad KD, Caporale N, et al. Inner limiting membrane barriers to AAV-mediated retinal transduction from the vitreous. *Mol Ther*. 2009;17:2096–2102.
38. Pfeiffer RL, Marc RE, Jones BW. Persistent remodeling and neurodegeneration in late-stage retinal degeneration. *Prog Retin Eye Res*. 2020;74:100771.
39. Marc RE, Jones BW. Retinal remodeling in inherited photoreceptor degenerations. *Mol Neurobiol*. 2003;28:139–147.
40. van Wyk M, Pielecka-Fortuna J, Lowel S, Kleinlogel S. Restoring the ON switch in blind retinas: Opto-mGluR6, a next-generation, cell-tailored optogenetic tool. *PLoS Biol*. 2015;13:e1002143.
41. Lu Q, Ganjawala TH, Krstevski A, Abrams GW, Pan ZH. Comparison of AAV-mediated optogenetic vision restoration between retinal ganglion cell expression and ON bipolar cell targeting. *Mol Ther Methods Clin Dev*. 2020;18:15–23.
42. Humayun MS, Prince M, de Juan E, Jr., et al. Morphometric analysis of the extramacular retina from postmortem eyes with retinitis pigmentosa. *Invest Ophthalmol Vis Sci*. 1999;40:143–148.
43. Jacobson SG, Sumaroka A, Aleman TS, Cideciyan AV, Danciger M, Farber DB. Evidence for retinal remodelling in retinitis pigmentosa caused by PDE6B mutation. *Br J Ophthalmol*. 2007;91:699–701.
44. Doroudchi MM, Greenberg KP, Liu J, et al. Virally delivered channelrhodopsin-2 safely and effectively restores visual function in multiple mouse models of blindness. *Mol Ther*. 2011;19:1220–1229.

Supplementary Material

Supplementary Video S1. Representative Y-maze test of Deino using her optogenetic gene therapy-treated left eye. (A) Her right eye is covered with an opaque contact lens. (B) Performance was recorded with infrared imaging so that the animal could be visualized while walking through the light-tight maze. The video is edited to clearly show the moment of decision where Deino decides to walk toward the light.